Heterogeneous Catalysis Hot Paper

DOI: 10.1002/ange.201402680

Design and Synthesis of Copper–Cobalt Catalysts for the Selective Conversion of Synthesis Gas to Ethanol and Higher Alcohols**

Gonzalo Prieto, Steven Beijer, Miranda L. Smith, Ming He, Yuen Au, Zi Wang, David A. Bruce, Krijn P. de Jong, James J. Spivey, and Petra E. de Jongh**

Abstract: *Combining quantum-mechanical simulations and synthesis tools allows the design of highly efficient CuCo/MoO_x catalysts for the selective conversion of synthesis gas ($CO + H_2$) into ethanol and higher alcohols, which are of eminent interest for the production of platform chemicals from non-petroleum feedstocks. Density functional theory calculations coupled to microkinetic models identify mixed Cu–Co alloy sites, at Co-enriched surfaces, as ideal for the selective production of long-chain alcohols. Accordingly, a versatile synthesis route is developed based on metal nanoparticle exsolution from a molybdate precursor compound whose crystalline structure isomorphically accommodates Cu^{2+} and Co^{2+} cations in a wide range of compositions. As revealed by energy-dispersive X-ray nanospectroscopy and temperature-resolved X-ray diffraction, superior mixing of Cu and Co species promotes formation of CuCo alloy nanocrystals after activation, leading to two orders of magnitude higher yield to high alcohols than a benchmark CuCoCr catalyst. Substantiating simulations, the yield to high alcohols is maximized in parallel to the CuCo alloy contribution, for Co-rich surface compositions, for which Cu phase segregation is prevented.*

Nanosized bimetallic particles bear great interest as functional materials for several emerging technologies.[1] As catalysts, they play a pivotal role in the realization of novel, "greener" chemical processes.[2–7] The synergistic combination of two metals represents an efficient approach towards original catalytic properties by either the creation of hybrid sites or the concerted action of concomitant functionalities. Bimetallic nanocatalysts also hold promise to replace monometallic catalysts based on precious, scarce metals by equally active and selective catalysts constituted of abundant and inexpensive metals.[8]

To reduce the dependence of our society on dwindling crude oil reserves, the rational design of solid catalysts for the selective conversion of synthesis gas (syngas, $CO + H_2$), derived from natural gas or lignocellulosic biomass feedstocks, into valuable products is currently considered a major scientific target.[9–11] The synthesis of ethanol and longer chain (C_{2+}) linear alcohols stands out as a catalytic route of eminent interest, owing to the relevance of these compounds as hydrogen carriers and fuels, precursors for important platform chemicals such as olefins, and reagents in the synthesis of plasticizers and detergents.[12–15] Moreover, the reaction is a prime example of those requiring synergy between proximate catalytic sites with different functionality, as both the dissociative activation and the non-dissociative insertion of CO are needed to produce high alcohols. Unlike for the Cu-catalyzed conversion of syngas to methanol or for the Fischer–Tropsch synthesis of hydrocarbons with Co or Fe catalysts, developing solid catalysts displaying sufficient selectivity and yields to realize the commercial-scale selective synthesis of C_{2+} alcohols remains a major challenge.

Rh is the only single metal able to selectively produce high alcohols by CO hydrogenation,[12,16,17] however, its high cost and limited availability exclude its application in large-scale processes of syngas conversion. As an alternative, bimetallic catalysts, for example, CuCo, CuFe or RuMo, have been proposed.[18–22] However, the nature of the active sites responsible for the production of C_{2+} alcohols and how to maximize their occurrence remain unclear. Although intimate contact between the metal components has been recognized as important to achieve a satisfactory selectivity,[23,24] catalyst preparation methodologies generally result in metal segregation, typically the formation of copper oxide during thermal activation treatment,[22c,23,25,26] which limits metal intimacy.

Here we adopt a combined approach, building on computational design and controlled synthesis methods to develop highly efficient bimetallic Co–Cu catalysts for the selective conversion of syngas to ethanol and higher alcohols. Simulations based on density functional theory (DFT) coupled to a microkinetic model[27] were employed to identify the preferred metal sites and optimum composition to selectively produce high alcohols by CO hydrogenation. To this end, we simulated the product selectivity pattern for the

[*] Dr. G. Prieto, S. Beijer, Y. Au, Prof. K. P. de Jong, Prof. P. E. de Jongh
Inorganic Chemistry and Catalysis
Debye Institute for Nanomaterials Science, Utrecht University
3584 CG, Utrecht (The Netherlands)
E-mail: p.e.dejongh@uu.nl
Dr. M. L. Smith, Z. Wang, Prof. J. J. Spivey
Cain Department of Chemical Engineering
Lousiana State University
Baton Rouge, LA 70803 (USA)
Dr. M. He, Prof. D. A. Bruce
Department of Chemical and Biomolecular Engineering
Clemson University
Clemson, SC 29634 (USA)

[**] This work was supported by the Center for Atomic-Level Catalyst Design, an Energy Frontier Research Center funded by the U.S. Department of Energy, Office of Science, Office of Basic Energy Sciences under Award Number DE-SC0001058. The authors acknowledge H. Meeldijk, G. Wang and M. Versluijs (UU) for STEM/EDX, UV/Vis and in situ XRD and SEM/EDX measurements and J. P. Holgado (ICMS-CSIC) for XPS experiments.

Supporting information for this article is available on the WWW under http://dx.doi.org/10.1002/anie.201402680.

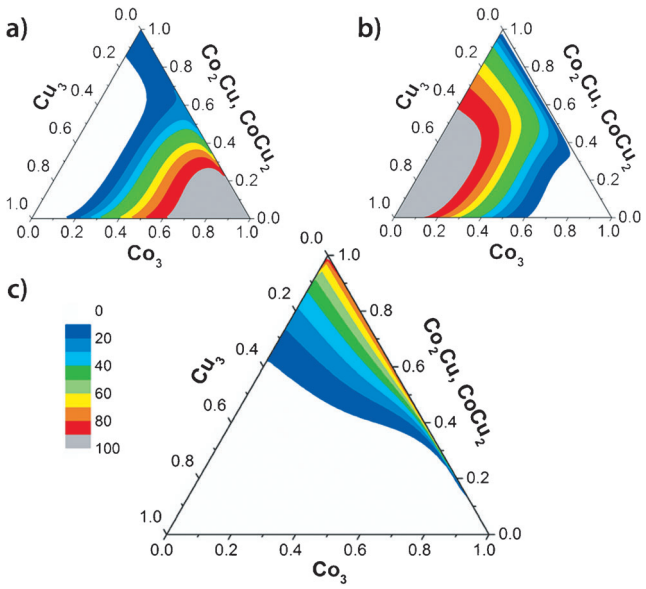

Figure 1. Selectivity (mol%) to a) CH_4, b) methanol, and c) ethanol as a function of the proportion of monometallic Cu, Co, and bimetallic CuCo surface sites as predicted by DFT calculations and microkinetic modelling.

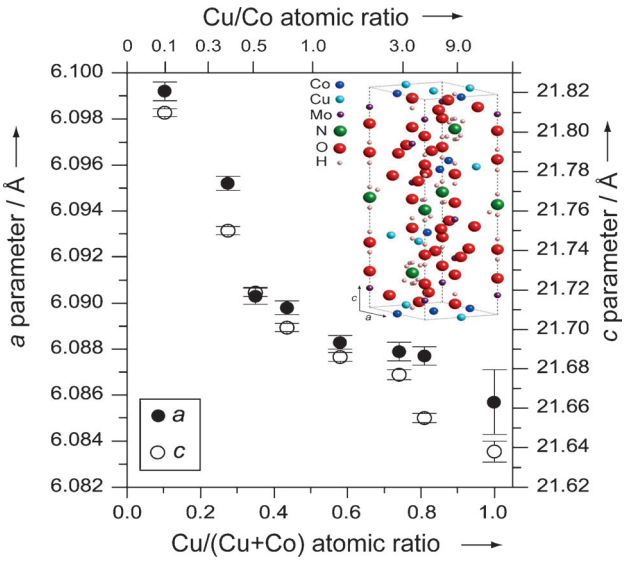

Figure 2. Evolution of the unit cell parameters for the metal ammonium molybdate ($R\bar{3}m$) precursor compound as a function of the catalyst composition. The inset shows a model of the proposed crystalline structure.

full range of possible surface compositions (Co_xCu_y) of a bimetallic metal cluster.

Figure 1 summarizes the results of the simulations (see Computational Methods in the Supporting Information). The selectivities to methane, as representative for the hydrocarbon products, methanol, and ethanol as a model high alcohol, are plotted as a function of the proportion of three possible surface sites, i.e. monometallic Cu_3 and Co_3, and bimetallic CuCo sites ($CuCo_2$ or Cu_2Co sites). Monometallic Co_3 and Cu_3 sites favor the formation of hydrocarbons (methane) and methanol, respectively, as has been established experimentally. Methanol is also predicted to be a major product when monometallic Cu_3 sites coexist with mixed CuCo sites. In this case, surface diffusion of CH_3 intermediates results in increased methanol production also on the bimetallic sites, highlighting the importance of considering migration of intermediate species between neighboring sites to predict product selectivity. A maximum selectivity to ethanol is predicted for a catalyst surface essentially free from pure Cu_3 sites, which displays a maximum contribution from mixed CuCo sites, that is, in alloy phases. Hence, the ideal catalyst surface to selectively produce C_{2+} alcohols is predicted to be a CuCo alloy phase for Co-rich compositions, for which no segregated Cu atom ensembles exist.

Based on these predictions, we have developed a novel synthesis route for CuCo catalysts aiming at superior alloy formation. Our approach relies on the identification of a crystalline compound whose lattice is flexible enough to accommodate Cu^{2+} and Co^{2+} at equivalent positions, providing the platform to achieve superior intimacy between the two metals upon their exsolution in the form of nanoparticles during subsequent activation treatments. Mixed metal ammonium molybdate compounds were synthesized by co-precipitation in an ammonia-alkalinized solution. The compounds were labeled CuCoMo(δ), where $\delta = 0$–1 represents the Cu/(Cu+Co) atomic ratio (Figure S1 in the Supporting Information). X-ray diffraction (XRD) patterns of all Cu-containing samples correspond to the trigonal $R\bar{3}m$ lattice of a layered metal ammonium molybdate (Figures S2 and S3).[28] As shown in Figure 2, the hexagonal unit cell shrinks systematically on increasing the copper content, in agreement with the smaller ionic diameter of Cu^{2+} as compared to high-spin Co^{2+} cations (Figure S2b). This provides direct support for the isomorphic substitution of the two metal cations in the crystalline lattice of the layered precursor compound for the full compositional range.

After decomposing this precursor by heating in air, metal molybdate crystalline structures are obtained, chiefly the triclinic ($P\bar{1}$) and monoclinic ($C2/m$) lattices characteristic of the monometallic $CuMoO_4$ and $CoMoO_4$ compounds. Their molar proportion varies continuously with catalyst composition, whereas the crystal lattice parameters are in agreement with isomorphic substitution of Cu^{2+} and Co^{2+} cations in all the identified molybdate compounds also after air-calcination (Figure S4). Scanning electron microscopy coupled to energy-dispersive X-ray spectroscopy (SEM-EDX) confirms a uniform distribution of both metals within each molybdate compound (Figure S5). A notably different microstructure is found for an air-calcined reference CuCoCr catalyst synthesized according to state-of-the-art procedures.[18] In this case, a separate CuO crystalline phase is found (Figure S6), in line with literature results.[23] This reference catalyst shows a macroporous, spatially inhomogeneous structure (Figure S6).

For selected samples with similar Cu/(Cu+Co) ratio of 0.51–0.58, the nanospatial distribution of Cu and Co was further investigated with EDX spectroscopy on ultrathin sections of the samples after air-calcination. As given in

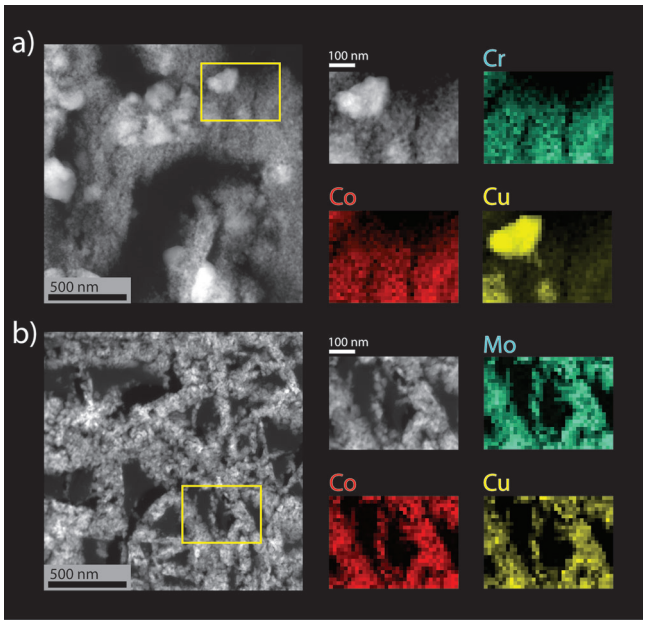

Figure 3. HAADF-STEM micrographs and elemental EDX maps (from the yellow box regions) for ultramicrotomed sections (80 nm thick) of a) the CuCoCr reference catalyst with (Cu/Cu + Co) = 0.51; and b) a CuCoMo catalyst with (Cu/Cu + Co) = 0.58 obtained from a crystalline ammonium molybdate precursor, after air-calcination.

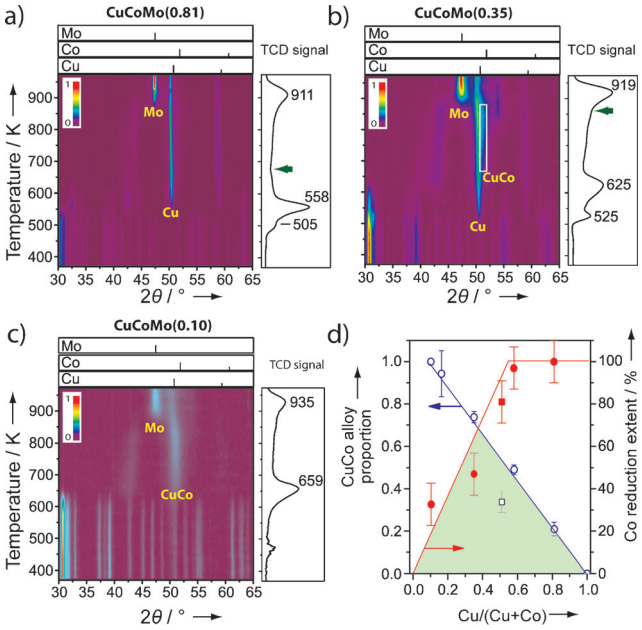

Figure 4. Temperature-resolved X-ray diffraction patterns and H_2 consumption profiles during the in situ reduction of CuCoMo catalysts with a Cu/(Cu+Co) atomic ratio of a) 0.81, b) 0.35, and c) 0.10. Green arrows indicate the temperatures at which the accumulated H_2 consumption corresponds to full reduction to Cu^0 and Co^0, alongside partial reduction of Mo^{6+} to Mo^{4+}. d) Evolution of the contribution of CuCo alloy within the crystalline metal phases (see also Figure S8), and the cobalt surface extent of reduction determined with X-ray photoelectron spectroscopy (Table S1), as a function of catalyst composition for as-reduced CuCoMo catalysts (circles) and the reference CuCoCr catalyst (squares).

Figure 3, for the reference CuCoCr, large (50–150 nm) CuO aggregates are found, within a matrix of a nanosized Cu–Co–Cr mixed oxide which is significantly depleted in copper with respect to the overall catalyst composition. In marked contrast, very uniform nanospatial distributions of Cu, Co and Mo are observed in the case of the CuCoMo catalyst obtained by decomposition of an ammonium metal molybdate precursor. Hence, the novel synthesis route provides superior mixing of Cu and Co which, unlike for the conventional preparation procedure, is preserved after the air-calcination thermal treatment.

Exsolution of Cu and Co from the oxide precursor compound, as supported nanocrystals, is achieved by reduction in H_2. The reducibility of the oxidic precursor has a large impact on the nature of the metal species after catalyst activation. Hence, selected CuCoMo catalysts were also investigated with temperature-resolved X-ray diffraction during in situ reduction. On heating the monometallic CuMo oxide in flow of 5 % H_2/He, decomposition of the starting copper molybdate and crystallization of Cu^0 occurs at 500–600 K (Figure S7).

Quantification of the H_2 consumption indicates that not only Cu but also reduction of Mo^{6+} to Mo^{4+} has occurred at 673 K. After formation of Cu crystallites, the resulting Mo^{IV} oxide (support) exhibits a rather amorphous character, as indicated by the absence of well-defined diffractions for Mo compounds up to 800 K, at which temperature further reduction to Mo^0 takes place. On the contrary, Co^{2+} is not easily reduced in the CoMo counterpart. No metallic Co^0 crystallites are detected up to 973 K, which is the maximum temperature studied (Figure S7).

For CuCoMo catalysts, the reduction behavior is qualitatively similar to that of the monometallic CuMo material (Figure 4). The H_2 consumption profiles indicate that reduction of Co^{2+} begins already at temperatures < 600 K, likely catalyzed by H_2 dissociation on nascent Cu^0 clusters. Nevertheless, no diffractions for Co^0 are detected, not even for > 20 wt % Co loadings. Despite the very low miscibility of bulk Cu^0 and Co^0, the formation of nanosized alloys has been previously proposed.[20,29] For our CuCoMo catalysts, alloying is indicated by the development of broad diffraction lines detected at d-spacing values intermediate between those characteristic of Cu^0 and Co^0 face-centered cubic (fcc) lattices. These features contribute as shoulders on the Cu^0 diffractions for Cu/(Cu+Co) ratios ≥ 0.16 (white frame in Figure 4b), but dominate for lower Cu contents (Figure 4c). This diffraction signal grows in intensity and progressively shifts to higher angles, indicating a decrease in d-spacing, on increasing the temperature in the range of 600–850 K, in agreement with cobalt incorporation as reduction of Co^{2+} species proceeds. Hence, these features indicate the formation of nanosized CuCo alloy phases upon metal exsolution from the molybdate precursor.

Based on these insights, a temperature of 673 K was selected for the reduction treatment preceding catalysis. In the activated CuCoMo catalysts, the relative contribution of the CuCo alloy phase within the metallic crystalline species decreases continuously with the Cu content (Figure 4d). A

reverse trend is observed for the reduction extent of Co species in the Cu/(Cu+Co) range of 0–0.5.

Hence, a maximum occurrence of the CuCo alloy phase is inferred at a Cu/(Cu+Co) ratio of ca. 0.35 (Cu/Co ≈ 1/2), representing the optimal balance between cobalt reducibility and Cu content (see shaded region in Figure 4d). Copper in surplus to what can be effectively alloyed with the reduced Co species segregates as large Cu crystallites at higher Cu/(Cu+Co) ratios, as revealed by HAADF-STEM (Figure S9). CuCoMo catalysts derived from layered molybdate compounds show a notably higher alloy contribution than for the reference CuCoCr. This result highlights the relevance of preventing phase segregation in the oxide precursors, by the novel synthesis route, to maximize the formation of nanosized alloy phases upon metal exsolution during a reduction treatment.

The catalytic performance of the CuCoMo materials was evaluated after incorporation of K as promoter, to enable direct comparison with the K-CuCoCr catalyst (Figure 5).

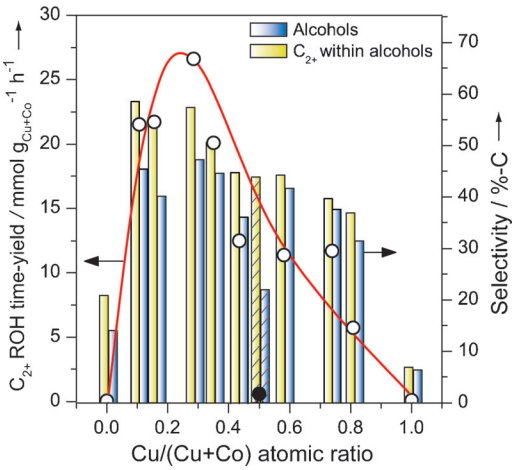

Figure 5. Evolution of the C_{2+} alcohols (ROH) time-yield and the CO_2-free selectivity to alcohols (both on a carbon molar basis) as a function of catalyst composition for the series of K-CuCo/MoO_x catalysts (open circles and solid bars) and the reference K-CuCo/CrO_x catalyst (full circle and dashed bars). The red line serves as a guide to the eye. Reaction conditions: $T = 543$ K, $P = 40$ bar, $H_2/CO = 1$, $X_{CO} < 2\%$. The concomitant water-gas shift reaction resulted in CO_2 selectivities of 22.4–41.6%.

The reference catalyst shows a total alcohol selectivity of 22%, 44% of which corresponds to higher alcohols. The time yield to C_{2+} alcohols is 0.35 mmol g_{Cu+Co}^{-1} h^{-1}. Similar high alcohols time yields in the range of 0.2–1.5 mmol g_{Cu+Co}^{-1} h^{-1} can be derived at 543 K for previously reported CuCo-based catalysts obtained by coprecipitation, electrodeposition, or metal oxalate decomposition.[22] As depicted in Figure 5, CuCoMo catalysts obtained by the novel route showed a superior activity and selectivity to high alcohols. At a Cu/(Cu+Co) ratio of 0.3 the selectivity to ethanol and higher alcohols was maximum, while the yield of C_{2+} alcohols reached 27 mmol g_{Cu+Co}^{-1} h^{-1}, ca. two orders of magnitude higher than for the K-CuCoCr reference catalyst. Interestingly, the optimal catalyst composition agrees well with the maximum occurrence of the nanosized CuCo alloy phase, upon prevention of Cu segregation (Figure 4d). Hence, our experimental results concur with the predictions by theory and suggest alloy-type mixed Cu–Co sites, in metal surfaces slightly enriched in Co, as responsible for the selective production of C_{2+} alcohols from synthesis gas.

In summary, the superior nanoscale metal intimacy achieved by the isomorphic substitution of Cu^{2+} and Co^{2+} cations in the crystalline lattice of a layered ammonium metal molybdate precursor is preserved after air-decomposition and promotes the formation of CuCo alloy nanocrystallites after catalyst reduction. In agreement with our predictions by DFT and microkinetic modeling, improved metal mixing in nanometric alloys, and prevention of Cu phase segregation, greatly boost the selectivity and yield towards C_{2+} alcohols. Future optimization of promoter(s) content and activation procedures are expected to result in additional improvements in catalytic performance.

Developing efficient catalysts for the selective production of high alcohols by CO hydrogenation, this study illustrates the relevance of combining quantum-mechanical calculations and microkinetic modeling with precise synthesis tools to design bimetallic catalysts. Besides, by providing structural uniformity in a wide range of compositions, the versatile synthesis route presented is promising for further structure–performance investigations in catalysts and other functional nanostructures where intimacy between two metals is essential, such as fuel cell electrodes and batteries.

Experimental Section

For DFT calculations, an icosahedral Co_7Cu_6 nanocluster was selected as the model to test the catalytic properties of various surface mono- and bimetallic metal sites. All electronic structure calculations were performed using Jaguar 7.7 at the density functional theory level. Carbon and oxygen atoms were described by the standard all-electron 6-31G** basis set. The diffusion behaviors of intermediate species were studied by the CI-NEB method. Microkinetic models were built taking into account reaction and diffusion steps on different sites. Cu–Co ammonium molybdate catalyst precursors were synthesized by co-precipitation from aqueous solutions of the metal nitrate precursors and ammonium hydroxide at a constant temperature of 363 K. A reference CuCoCr catalyst was prepared according to preferred embodiments described in the patent literature.[18b] Catalytic tests were carried out in fixed-bed flow reactor at differential CO conversion levels after in situ reduction in 20% H_2/Ar flow. More details on the computational and synthesis methods, characterizations and catalytic tests are given in the Supporting Information.

Received: February 21, 2014
Published online: May 14, 2014

Keywords: alloy nanoparticles · CO hydrogenation · heterogeneous catalysis · high alcohols · supported catalysts

[1] R. Ferrando, J. Jellinek, R. L. Johnston, *Chem. Rev.* **2008**, *108*, 845–910.
[2] a) J. K. Edwards, G. J. Hutchings, *Angew. Chem.* **2008**, *120*, 9332–9338; *Angew. Chem. Int. Ed.* **2008**, *47*, 9192–9198; b) M.

Sankar, N. Dimitratos, P. J. Miedziak, P. P. Wells, C. J. Kiely, G. J. Hutchings, *Chem. Soc. Rev.* **2012**, *41*, 8099 – 8139.
[3] Y. Román-Leshkov, C. J. Barrett, C. Y. Liu, J. A. Dumesic, *Nature* **2007**, *447*, 982 – 985.
[4] D. A. Hansgen, D. G. Vlachos, J. G. Chen, *Nat. Chem.* **2010**, *2*, 484 – 489.
[5] Q. Zhai, S. Xie, W. Fan, Q. Zhang, Y. Wang, W. Deng, Y. Wang, *Angew. Chem.* **2013**, *125*, 5888 – 5891; *Angew. Chem. Int. Ed.* **2013**, *52*, 5776 – 5779.
[6] N. E. Kolli, L. Delannoy, C. Louis, *J. Catal.* **2013**, *297*, 79 – 92.
[7] G. H. Wang, J. Hilgert, F. Richter, F. Wang, H.-J. Bongard, B. Spliethoff, C. Weidenthaler, F. Schüth, *Nat. Mater.* **2014**, *13*, 293 – 300.
[8] a) F. Studt, F. Abild-Pedersen, T. Bligaard, R. Z. Sørensen, C. H. Christensen, J. K. Nørskov, *Science* **2008**, *320*, 1320 – 1322; b) M. Armbrüster, K. Kovnir, M. Friedrich, D. Teschner, G. Wowsnick, M. Hahne, P. Gille, L. Szentmiklósi, M. Feuerbacher, M. Heggen, F. Girgsdies, D. Rosenthal, R. Schlögl, Y. Grin, *Nat. Mater.* **2012**, *11*, 690 – 693.
[9] A. Y. Khodakov, W. Chu, P. Fongarland, *Chem. Rev.* **2007**, *107*, 1692 – 1744.
[10] G. L. Bezemer, J. H. Bitter, H. P. C. E. Kuipers, H. Oosterbeek, J. E. Holewijn, X. Xu, F. Kapteijn, A. J. van Dillen, K. P. de Jong, *J. Am. Chem. Soc.* **2006**, *128*, 3956 – 3964.
[11] H. M. T. Galvis, J. H. Bitter, C. B. Khare, M. Ruitenbeek, A. I. Dugulan, K. P. de Jong, *Science* **2012**, *335*, 835 – 838.
[12] X. Pan, Z. Fan, W. Chen, Y. Ding, H. Luo, X. Bao, *Nat. Mater.* **2007**, *6*, 507 – 511.
[13] J. J. Spivey, A. Egbebi, *Chem. Soc. Rev.* **2007**, *36*, 1514 – 1528.
[14] V. Subramani, S. K. Gangwal, *Energy Fuels* **2008**, *22*, 814 – 839.
[15] M. Gupta, M. L. Smith, J. J. Spivey, *ACS Catal.* **2011**, *1*, 641 – 656.
[16] Y. Choi, P. Liu, *J. Am. Chem. Soc.* **2009**, *131*, 13054 – 13061.
[17] G. Prieto, P. Concepción, A. Martínez, E. Mendoza, *J. Catal.* **2011**, *280*, 274 – 288.
[18] a) P. Courty, D. Durand, A. Sugier, *J. Mol. Catal.* **1982**, *17*, 241 – 254; b) A. Sugier, E. Freund, U.S. Patent 4122110, **1987**.
[19] W. X. Pan, R. Cao, G. L. Griffin, *J. Catal.* **1988**, *114*, 447 – 456.
[20] J. Wang, P. A. Chernavskii, A. Y. Khodakov, Y. Wang, *J. Catal.* **2012**, *286*, 51 – 61.
[21] K. Xiao, X. Qi, Z. Bao, X. Wang, L. Zhong, K. Fang, M. Linc, Y. Sun, *Catal. Sci. Technol.* **2013**, *3*, 1591 – 1602.
[22] a) V. Mahdavi, M. H. Peyrovi, M. Islami, J. Y. Mehr, *Appl. Catal. A* **2005**, *281*, 259 – 265; b) M. Gupta, V. Schwartz, S. H. Overbury, K. More, H. M. Meyer, J. J. Spivey, *J. Phys. Chem. C* **2012**, *116*, 10924 – 10933; c) Y. Xiang, V. Chitry, P. Liddicoat, P. Felfer, J. Cairney, S. Ringer, N. Kruse, *J. Am. Chem. Soc.* **2013**, *135*, 7114 – 7117.
[23] X. Xiaoding, E. B. M. Doesburg, J. J. F. Scholten, *Catal. Today* **1987**, *2*, 125 – 170.
[24] R. M. Bailliard-Letournel, A. J. G. Cobo, C. Mirodatos, M. Primet, J. A. Dalmon, *Catal. Lett.* **1989**, *2*, 149 – 156.
[25] G. R. Sheffer, R. A. Jacobson, T. S. King, *J. Catal.* **1989**, *116*, 95 – 107.
[26] J. I. Di Cosimo, A. J. Marchi, C. R. Apesteguia, *J. Catal.* **1992**, *134*, 594 – 607.
[27] a) *Computational Catalysis* (Eds.: A. Asthagiri, M. J. Janik), *RSC*, Cambridge, **2014**; b) A. J. Medford, A. C. Lausche, F. Abild-Pedersen, B. Temel, N. C. Schjødt, J. K. Nørskov, F. Studt, *Top. Catal.* **2014**, *57*, 135 – 142.
[28] D. Levin, S. L. Soled, J. Y. Ying, *Inorg. Chem.* **1996**, *35*, 4191 – 4197.
[29] Q. Li, Q. Wang, D. Li, X. Lü, X. He, *J. Phys. Lett. A* **2008**, *372*, 6764 – 6769.

